Penerbit Akademia Baru

Journal of Advanced Research Design

Journal homepage:
https://akademiabaru.com/submit/index.php/ard
ISSN: 2289-7984

Computational Fluid Dynamics Simulations of Wind-Induced Ventilation in Idealized Step-Up Street Canyons

Muhammad Faris Hamzah[1], Ahmad Faiz Mohammad[1,*]

[1] Department of Mechanical Precision Engineering, Malaysia-Japan International Institute of Technology, Universiti Teknologi Malaysia, 54100 Kuala Lumpur, Malaysia

ARTICLE INFO

Article history:
Received 18 November 2020
Received in revised form 1 December 2020
Accepted 9 May 2021
Available online 10 May 2021

Keywords:
CFD; wind-induced ventilation; step-up canyon

ABSTRACT

In the urban environment, a street canyon that lies between two buildings is sheltered, to some degree, from wind flow. To enhance wind penetration into the street canyon, the step-up canyon made up of the lower upwind building and the higher downwind building, can be instead used. Computational fluid dynamics (CFD) simulations were performed using the Reynolds-averaged Navier Stokes (RANS) *k*- epsilon model to examine the wind flow characteristics in street canyons and obtain the ventilation rate, *Q* of window openings with the window-to-wall ratio (WWR) of 0.25 in various step-up canyons designs; the geometry of a step-up canyon is defined by the aspect ratio which is the ratio between the upwind building height to the downwind building height, *hu*/*hd*. The simulation results indicated that the increase of *hu*/*hd* from 0.25 to 1.0, corresponding to the increase of the upwind building height, led to the decrease of *Q*. The flow visualizations obtained from the CFD simulations showed the types of wind flow characteristics, such as deflected and recirculating flows, formed in the street canyon and affected the values of *Q*. In brief, the results indicated the feasibility of the step-up canyon, particularly with *hu*/*hd* = 0.25 and 0.50, in channelling wind flows into the canyon and increasing the ventilation rate of the building.

1. Introduction

Urban heat island (UHI) is a phenomenon where the temperature in an urban area is higher than the temperature in its surrounding area [16,20]. The UHI phenomenon is a universal problem affecting urban areas around the world [14]. Kuala Lumpur, a city characterized by a hot and humid weather all year round, is also prone to effects of the UHI phenomenon [2]. Additionally, other cities like Putrajaya and Singapore are also reported to have the UHI phenomenon [2,19].

In the urban environment, air temperature tends to stay at a higher level due to various factors. During the daytime, building and road surfaces are heated more quickly, thereby increasing the ambient temperature. Anthropogenic heat produced by human activities such as *via* transportation and indoor cooling system is also a factor of the UHI. The situation is worsened by lack of vegetation

* *Corresponding author.*
E-mail address: ahmadfaiz@utm.my

in the urban environment. Tree canopies can provide shade and cooling effect from solar heating. Without much vegetation, it is unlikely to reduce the UHI effect in the urban environment [2].

The build-up of heat in the urban environment cannot effectively escape due to the morphology of an urban area. In dense urban areas, buildings are relatively close to one another, inhibiting the air movement thus restricting its effectiveness of heat transport. To represent this situation better, consider a street canyon which is the region between two adjacent buildings. A street canyon is sheltered by the upwind building, blocking the air flow from entering it. The air flow can only skim over the buildings, creating a flow regime known as skimming flow [17]. As a result, only a weak, circulating flow can be generated inside the street canyon, as shown in Figure 1.

Due to skimming flow, ventilation induced by wind velocity, namely wind- induced ventilation in a street canyon, is minimized. This is mainly caused by building obstruction to the wind flow and the deficient distance between two adjacent tall buildings [11], this inhibits sufficient airflow between the buildings for wind-induced ventilation. Coupled with the UHI effect, air temperature in a street canyon can also increase. Consequently, the rise of urban air temperature leads to high energy consumption for cooling purposes in the building sector [9].

Therefore, the rising concern of UHI and increasing demand of energy, which is a consequence of urbanization, become the motivation of this research to investigate better and more sustainable urban designs. While improving the designs of existing cities seems impractical, better urban designs can be imposed on new urban developments. Hence, this research is focused on the fundamental aspect of urban design towards improvement of wind-induced ventilation in the urban environment.

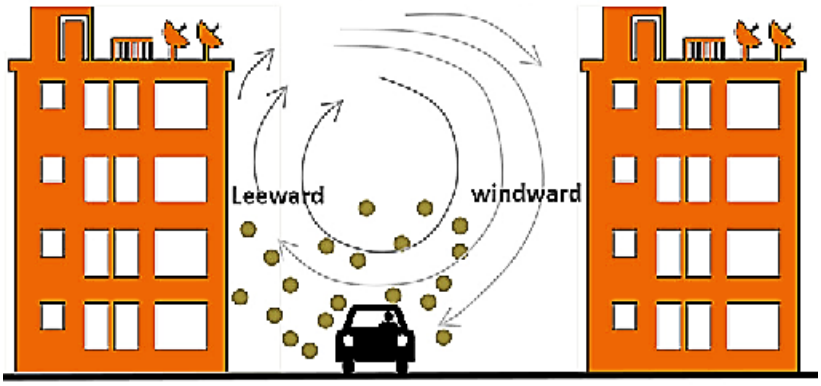

Fig. 1. Street canyon flow inhibited by two adjacent buildings

Street canyons in dense urban areas are typically sheltered from wind flows. Ideally, the building facing the head wind (i.e. upwind building) is lower than the building behind it (i.e. downwind building), creating a step-up street canyon design [1]. This design allows the taller downwind building to act as an obstacle to the free-stream wind flow that is subsequently directed into the street canyon; this would allow for an increased ventilation rate of the downwind building through its openings. Moreover, with the step-up design, the wind flow will be directed into the canyon and subsequently lead to better air circulation in the canyon.

The dimension of a street canyon is determined by the heights of the upwind and downwind buildings and the separation distance between them [6]. For a deep canyon, for which the heights of both buildings are equal, the aspect ratio which is the ratio of the upwind building height to the downwind building height is equal to unity. This is typically where skimming flow is observed. Therefore, it is essential to demonstrate how changing the street canyon's aspect ratio can influence wind-induced ventilation in the canyon region. Through the approach of computational fluid

dynamics (CFD), the investigation can be implemented for various street canyon configurations with idealized geometries i.e. without detailed geometric features [10].

Therefore, the aim of this research is to investigate the practicality of the step-up canyon configurations in optimizing the building's indoor ventilation. Additionally, in the event of highly turbulent flows, the step-up canyon design can also act as a shelter against strong wind forces. Since urban populations around the world, particularly in developing countries such as Malaysia and other Southeast Asian countries, are expected to continue growing [23], the proposed step-up canyon design will be of great importance towards future urban development and UHI mitigation strategies.

2. Literature Review

2.1 Urban Heat Island

UHI is a common phenomenon happening in urban areas around the globe where it is responsible for the higher ambient temperature in the urban areas than in the suburban areas [20]. This phenomenon is not a natural occurrence by nature however it is the product of human modification of the local climate [19,25]. The schematic of the UHI phenomenon is displayed in Figure 2.

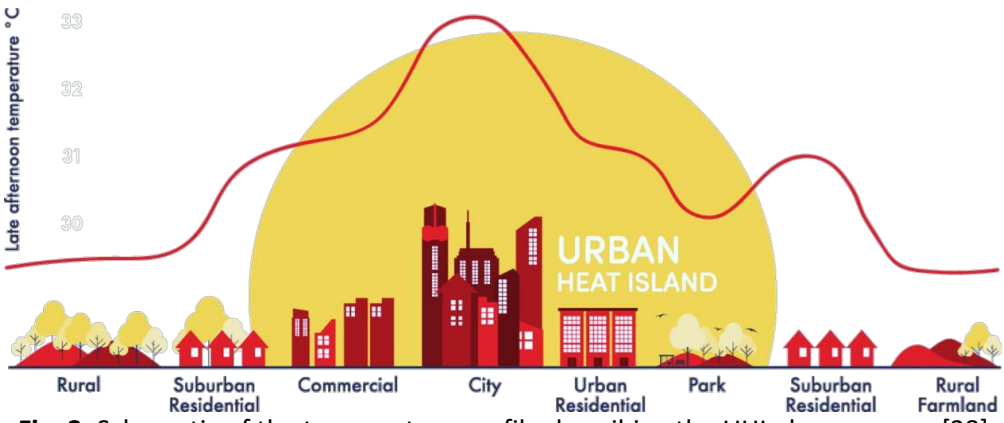

Fig. 2. Schematic of the temperature profile describing the UHI phenomenon [28]

UHI is a result of the increased temperature due to the absorbed long-wave radiation by the atmosphere which is reflected to the walls of the buildings and the street surfaces [15]. Besides that, materials used to build the buildings which act as the black body and absorb the solar heat during the day and emit heat through convection at night [16]. Lacking the coverage of vegetation in an urban area also contributes to UHI [14], trees, grass and other vegetation can essentially provide shade and evaporative cooling that reduce the air temperature. Internal combustion car emissions through the car exhaust produce a considerable amount of heat in the immediate surroundings deemed to be one of the causes of UHI [11]. Anthropogenic heat released from heated or cooled buildings is also one of the factors of the rise in the urban temperature [11]. Moreover, buildings in an urban area tend to obstruct the wind flow, reducing the wind speed. This leads to the lack of ventilation potential in an urban area. Consequently, hot air trapped between buildings has no transport mechanism as the wind loses its momentum for heat dispersion.

To a large extent, UHI is the result of human modification of the local climate. The modification of land by erecting tall buildings creates a microclimate with an impact on the quality of the environment around it. In particular, the local microclimate of a street canyon, which is a region that lies between two adjacent buildings, has changed significantly with the increase of temperature and the reduced wind speed.

The rise of temperature in the buildings and street canyons will significantly cause unpleasantness and thermal discomfort thus urban dwellers will look for temporary solutions. Higher temperature in an urban area leads to an increased demand on cooling loads thereby increasing the energy consumption of air conditioners [2,14]. The use of the air conditioner is not only expensive, but the notion of cooling a space while heating up the surrounding atmosphere is not sustainable and eco-friendly.

2.2 Wind Flow in the Urban Street Canyon

The wind environment in an urban area is influenced by many factors. The complex interaction of vertical velocity gradient, incident wind, turbulence and building shape, size and layout are factors that determine the wind flow behaviour and patterns. Obstruction to the wind flow due to the urban geometry is considered a limiting factor to the ventilation potential that the wind provides. To better understand the wind flow behaviour in an urban setting, a closer approach can be adopted, that is through the visualization of wind flow in the urban street canyon.

An urban street canyon is the space that is formed between two adjacent buildings. The aspect ratio of a street canyon is defined as the ratio of the building height to the width or distance between the two buildings. An urban street canyon can mainly act as an obstruction towards the upcoming wind flow to a certain degree at which it affects the temperature and air quality within the canyon. There are three basic flow regimes that are classified according to the aspect ratio of the canyon. Oke [17] showed that the isolated roughness flow happens in street canyons with the aspect ratio of < 0.30, wake interference flow 0.30-0.70 and skimming flow at > 0.70.

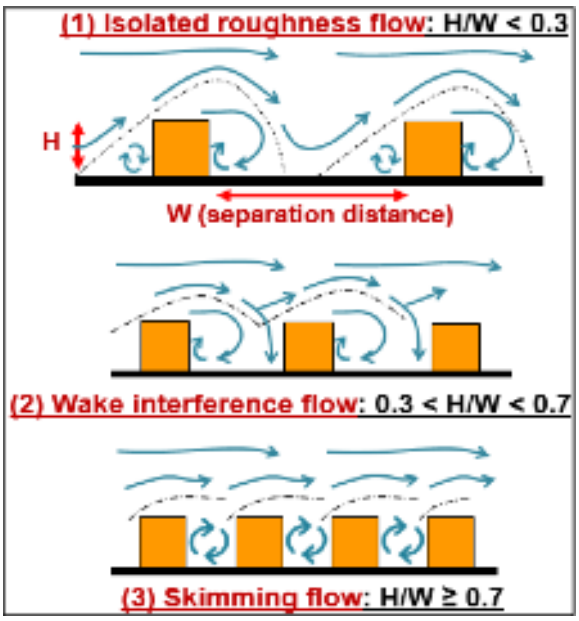

Fig. 3. Schematic of the three flow regimes observed in the street canyons [17]

The isolated roughness flow exists in the street canyon with $H/W < 0.3$. In this regime, the downwind building is not significantly sheltered by the upwind building. This flow regime is characterized by two separate vortices i.e. recirculating flows near respective buildings. The wake interference flow occurs in the street canyon with $0.3 < H/W < 0.7$. This is the condition whereby the deflected flow from the upwind building overlaps with the downwind building.

Last but not least, skimming flow is typically observed in deep and narrow street canyons wherein the aspect ratio is large due to the tall building height. The wind skims the top of the two buildings and only a significant amount of air flow is diverted into the canyon, consequently reducing the potential of wind circulation in the canyon. This is not conducive for the building's indoor ventilation which is explained in the next section. In fact, less ventilation inside the canyon also leads to heat and pollutant trapping.

2.3 Indoor Ventilation

Indoor ventilation is necessary to provide a cooling effect to occupants and air circulation in the indoor space. An indoor space can be naturally ventilated or mechanically ventilated. For the latter, electric fans and air conditioners are typically used in tropical climate. A more advanced mechanical ventilation system known as the heating, ventilation and air-conditioning (HVAC) system is often used in urban buildings; however, it is found to consume 68 % of the energy in service and residential buildings by a study by Orme [18]. The ventilation indoor is either from a HVAC system or natural ventilation from wind flow and buoyancy [8].

There are two main driving mechanisms of indoor ventilation, wind induced and thermal buoyancy. Wind-induced ventilation is induced by having different pressures between the inside and outside of a building. A greater difference between the indoor and outdoor pressures essentially leads to better ventilation potential in an indoor space [13,26]. The pressure on the surface of the building heavily relies on the building opening size (i.e. window), represented by the window-to-wall ratio (WWR), the shape of the opening and the position of the opening. On the other hand, the difference on the buoyancy of the cool and warm air inside the building creates a thermal buoyancy ventilation effect [12]. As air temperature rises, its density decreases, creating a difference in buoyancy; warmer air will rise and escape through the roof or the higher opening. This allows the indoor space to be naturally ventilated.

In addition, there are two main types of indoor ventilation, namely single-sided ventilation and cross ventilation. By implementing an opening in the direction of the wind, wind flow will enter and exit through the opening of the building; this is called single-sided ventilation [4,7]. On the other hand, cross ventilation requires two openings, in the windward and leeward sides of a building. This allows the inflow and outflow of air, each through the two opening in the opposite sides of the building [21,24]. However, wall porosity, surrounding obstacles and building geometry largely impact the efficiency of wind-induced indoor ventilation.

2.4 Mode of Investigation

The interaction between buildings and wind flows is typically studied using any of the three methods of the wind flow described as follows:

i. Wind tunnel experiment - A measurement technique of air flow properties in a wind tunnel equipped with measuring instruments.
ii. CFD simulation - A computational technique of solving flow-related problems.
iii. Field measurement - A data collection technique of real-time airflow properties using tools and instruments.

CFD is a numerical method of studying fluid properties and motions using computer software or applications such as Open Source Field Operation and Manipulation (OpenFOAM®), ANSYS Fluent

and STAR- CD. Major advantages of CFD are in terms of complementing analytical findings of wind tunnel experimentation and reducing the research effort required for both experimental and field measurement studies.

In this research, OpenFOAM®, was used to perform all CFD simulations. OpenFOAM® provides flexibility to users as its source code is written using the C++ programming language, covering a large set of codes stored in numerous libraries for multiple applications and case studies.

3. Methodology

The techniques applied to perform CFD simulations using the OpenFOAM® Version 7 software are provided in detail. Figure 4 shows the flowchart of the methodology in this research.

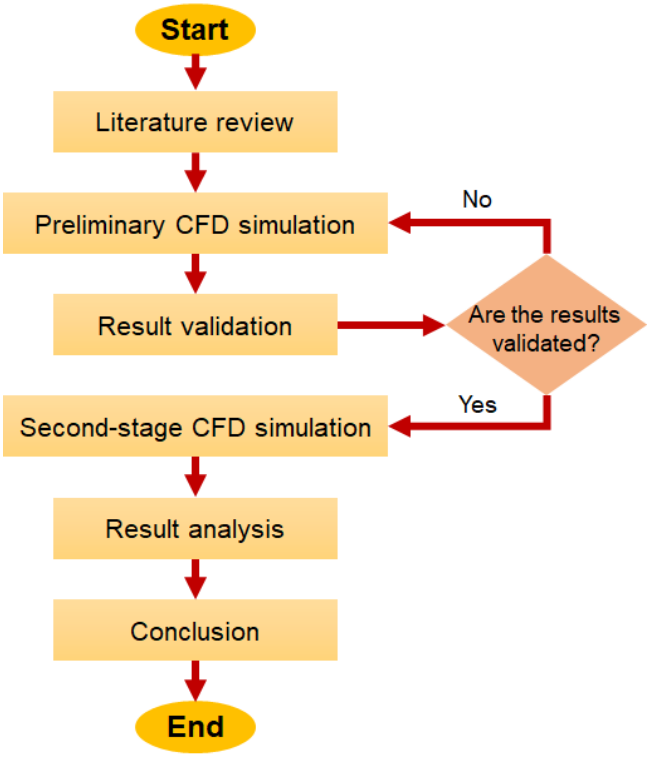

Fig. 4. Research flowchart

3.1 Preliminary CFD Simulation

3.1.1 Pre-processing stage

The first stage of the simulation is the pre-processing stage which involves setting up simulation parameters and constructing the models. Construction of a 3D model of the buildings was done using the AutoCAD® software. The 3D model of the building has the same height, H and width and a thickness of a quarter of the height, w = 0.25H, which is identical to the model in the wind tunnel experiment of Tominaga *et al*., [22], following the CFD guidelines for urban wind study developed by the Architectural Institute of Japan [5]. It is important to maintain the same building dimensions for the purpose of validation.

The computational domain was constructed in OpenFOAM; the schematic of the computational domain is shown in Figure 5. The lengths of the domain in the streamwise (x), spanwise (y) and vertical (z) directions are 20H, 11H and 5H, respectively, according to the AIJ guidelines. The

downstream distance from the building is much longer to allow for fully developed turbulent wakes so as not to interfere with the flow around the building.

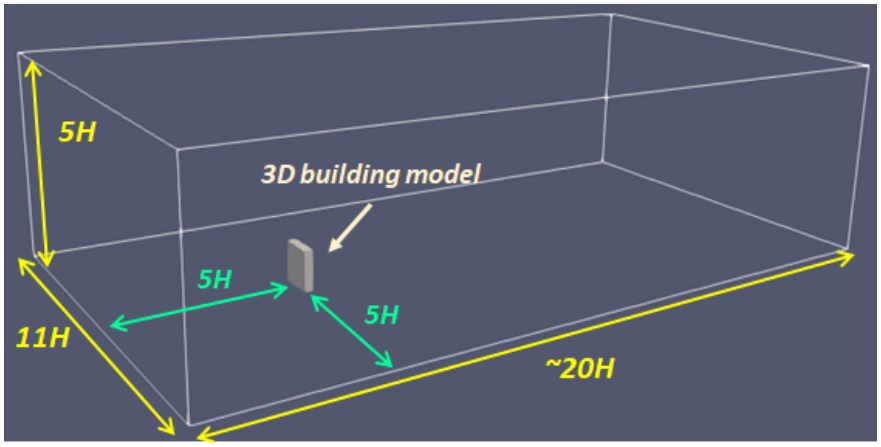

Fig. 5. Computational domain of the preliminary simulation

3.1.2 Boundary condition setting

Boundary conditions were applied to the computational domain with the purpose of simulating realistic wind flow with the effect of boundary layer. The boundary conditions applied are shown in Table 1.

Table 1
Boundary conditions applied in the computational domain

No.	Boundary of domain	Condition for velocity	Justification
1	Inlet	Power law profile	• To stimulate a realistic incoming wind flow in the domain based on a typical urban area • Initial velocity is based on the input velocity profile at the inlet
2	Outlet	Zero gradient	• To produce an outlet flow as a result of the developed internal flow
3	Top surface and lateral sides	Slip	• To allow for a fully-developed flow (freestream flow velocity of about 8 m/s)
4	Bottom surface and building surfaces	No-slip	• To generate a realistic boundary-layer flow induced by surface friction • Initial velocity is zero

At the building surfaces, the mesh size was configured to be finer as the flow structure in this region is smaller, as shown in Figure 6. This will allow a more accurate simulation of near-wall flows. Additionally, wall function was used on the domain's bottom surface and building surfaces to solve for near-wall flows more accurately. The use of the wall function eliminates the need for high mesh refinement in those regions, which would otherwise increase the total grid cells in the domain. The use of the wall function is an alternative for reducing the total simulation time and beneficial when the available computational capacity is limited.

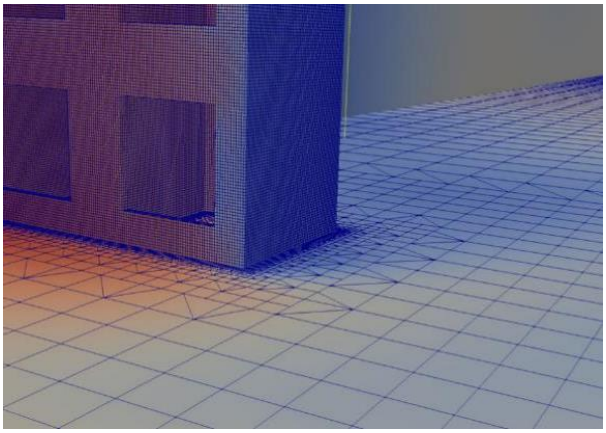

Fig. 6. Refined mesh distribution near the building

3.1.3 Turbulence model and flow condition

Turbulence modelling is an important approach in a CFD simulation. It represents the technique of solving the governing equations of fluid flows, namely the continuity and Navier-Stokes equations. The turbulence model used in this research was the Reynolds-averaged Navier-Stokes (RANS) *k*-epsilon model. This turbulence model is suitable for incompressible flows that are influenced by boundary-layer effect due to surface roughness. In fact, RANS is typically employed for analytical discussions on mean flow properties in several studies focused on fluid-structure interactions.

In terms of the flow condition, the RANS *k*-epsilon model is a suitable approach to solve incompressible flows. The Reynolds number, *Re*, which is the ratio between the inertial and viscous forces in the fluid flow, is 2.2 × 106, based on the building height and the reference freestream velocity of 8 m/s. The high *Re* indicates the development of turbulent flows, and thus the viscous effect in the flow can be neglected, which is possible when the flow is assumed to be incompressible.

3.1.4 Processing stage

The second stage is the processing stage wherein the simulation is run, and the convergence of the simulation is checked. Before the simulation was run, the computational domain was decomposed into 8 subdomains based on the number of processors used in the high-performance desktop workstation. The simulation was run using eight processors in parallel. Figure 7 shows the flowchart of simulation processing implemented in this research.

The simulation process started at 0 s and ended at 100 s, with the time interval of 0.1 s. The selection of the start and end times was arbitrary, but can be justified with the result of residual convergence presented in the next subsection. The residual data was recorded at each time step in a log file in each case folder. At the end of each simulation, the residuals were checked to determine if the solution was converged and reached a stable solution (i.e. remained at a constant value). If the results were not converging, the initial boundary settings and the time control settings will be reviewed and adjusted if needed before rerunning the simulation. The residuals of the data must be converged before the output data can be used for validation and analysis.

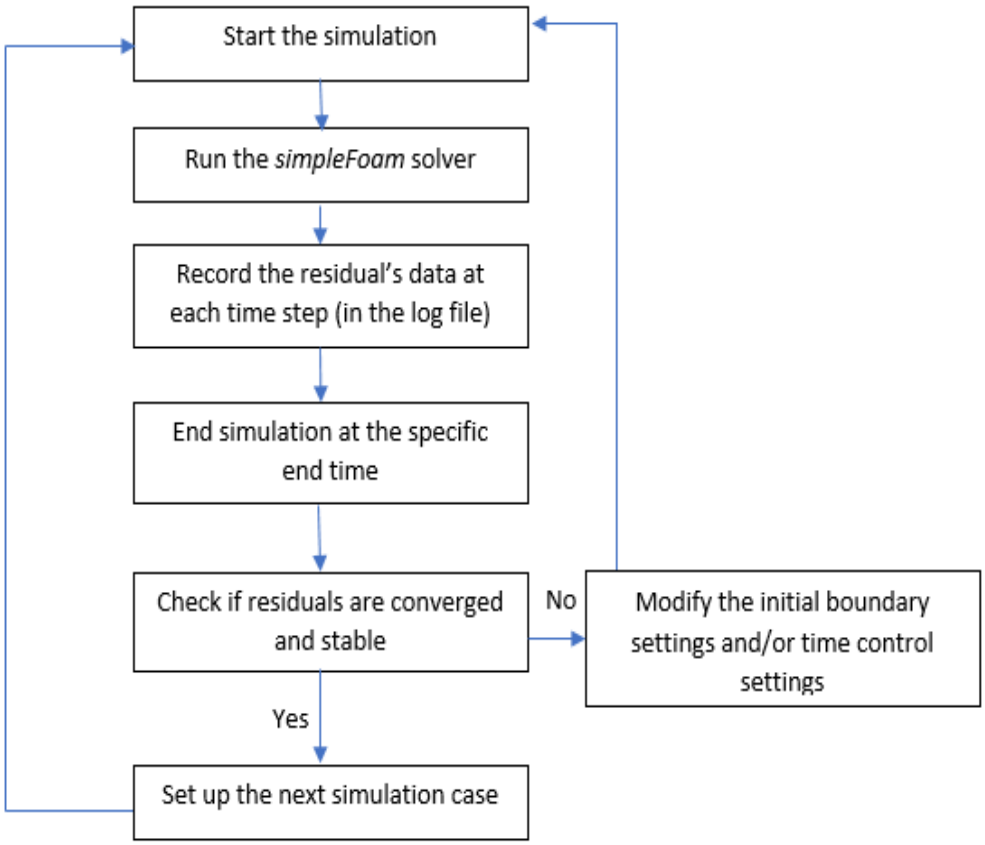

Fig. 7. Flowchart of simulation processing

3.1.5 Simulation convergence

The simulation was run based on the steady-state assumption of the flow. For this reason, the solver known as *simpleFoam* was adopted. This choice was made as the focus of this simulation was to obtain the time-independent solution of the flow, rather than fluctuations in the flow with respect to time. Besides, data validation and analysis required the use of the final output data from the simulations.

The residual data was extracted using the command *foamLog-n log* which saved the residual data into the case folder. The residual data of *Ux* (streamwise component of the velocity), *Uy* (spanwise component of the velocity) and *Uz* (vertical component of the velocity) are plotted against time of the simulation, from 0 to 30 s, to demonstrate the convergence of the residuals; these are shown in Figures 8, 9 and 10. All figures show that convergence was achieved from 15 s onwards until 30 s; in fact, due to the steady-state nature of the flow, the convergence was maintained until the end time i.e. 100 s. The simulation was continued until 100 s, despite the convergence observed much earlier, to ensure that the simulated flow was fully converged.

In principle, residual values represent numerical errors in the computational of a CFD simulation. As it reaches the convergence criteria of smaller than 10 - 5, the solution of the simulation has reached convergence. This step is crucial as it demonstrates that the numerical errors can be minimized.

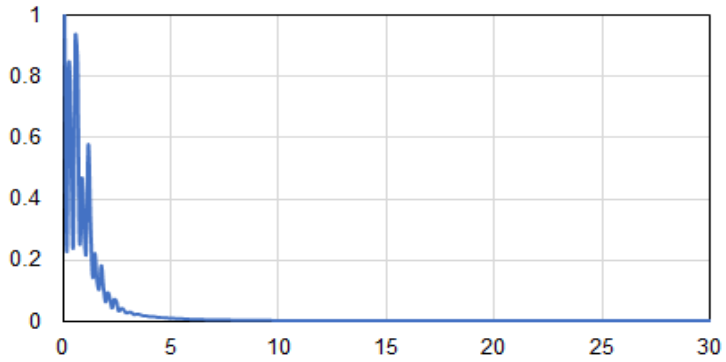

Fig. 8. Residual of velocity in the streamwise direction (*Ux*)

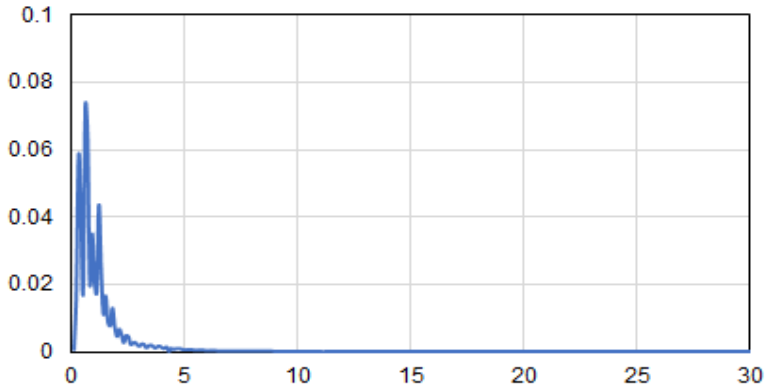

Fig. 9. Residual of velocity in the spanwise direction (*Uy*)

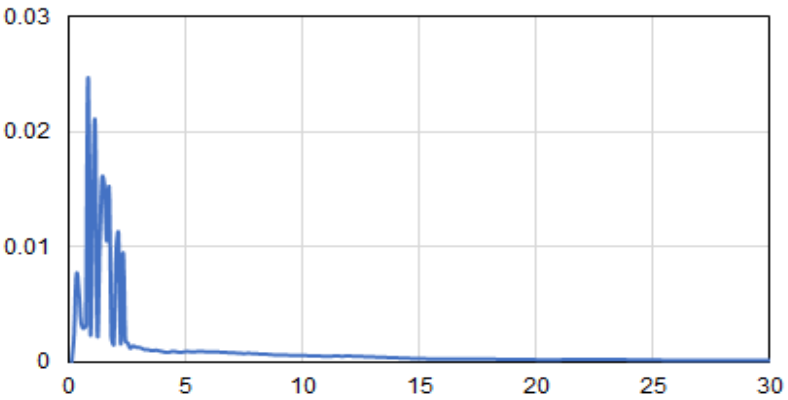

Fig. 10. Residual of velocity in the vertical direction (*Uz*)

3.2 Result Validation

Result validation is an important part of the preliminary CFD simulation. It is part of the post processing stage, involves data analysis and collection. The CFD simulation is validated against the published wind tunnel experimental (WT) data by AIJ [5]. The velocity profile was taken at the inlet of the computational domain, and plotted in Figure 11. The vertical axis is the normalized height where *h* is the building height and the horizontal axis is the normalized velocity where U_{ref} is the reference freestream velocity (8 m/s). The figure illustrates close agreement between the CFD and WT data, suggesting that the numerical and boundary settings applied are suitable to develop realistic, turbulent flows obtained in the wind tunnel experiment.

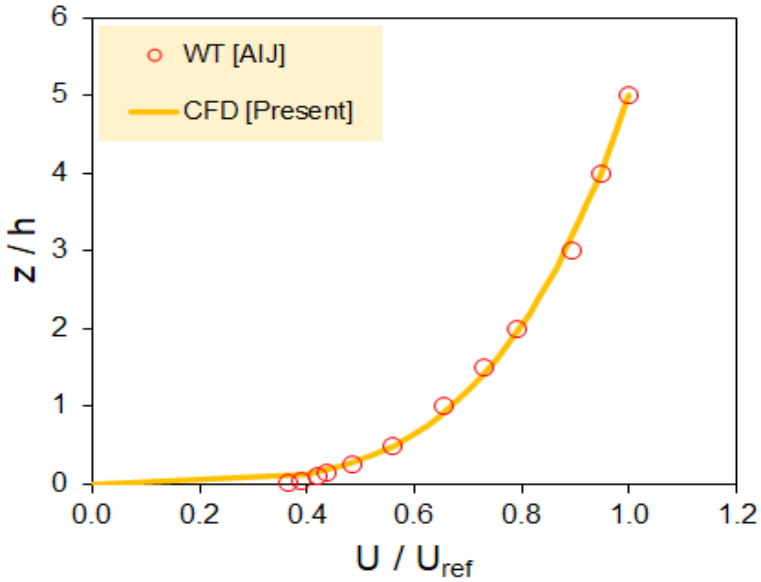

Fig. 11. Inlet velocity profiles of the present CFD simulation and the wind tunnel (WT) experiment from the AIJ database [5]

3.3 Mesh Sensitivity Analysis

As part of result validation, the mesh sensitivity analysis was performed using four different mesh refinement levels. Each refinement level varies in terms of the number of grid cells, as detailed out in Table 2. The range of the total number of cells is from 1.4 million up to 7.0 million grid cells. Mesh refinement is particularly critical near the building surface and openings; as an example, Figure 12 shows the mesh distribution near the building for the V2 level.

Table 2
Mesh refinement levels for the sensitivity analysis

Refinement level	Number of grid cells					
	Δx	Δy	Δz	Per building width, *w*	At the opening (*y* x *z*)	Total
V1	160	88	40	16	10 x 10	1 389652
V2	160	88	56	16	10 x 20	2 383252
V3	160	88	56	32	20 x 40	4 947548
V4	160	132	56	32	30 x 40	7 027244

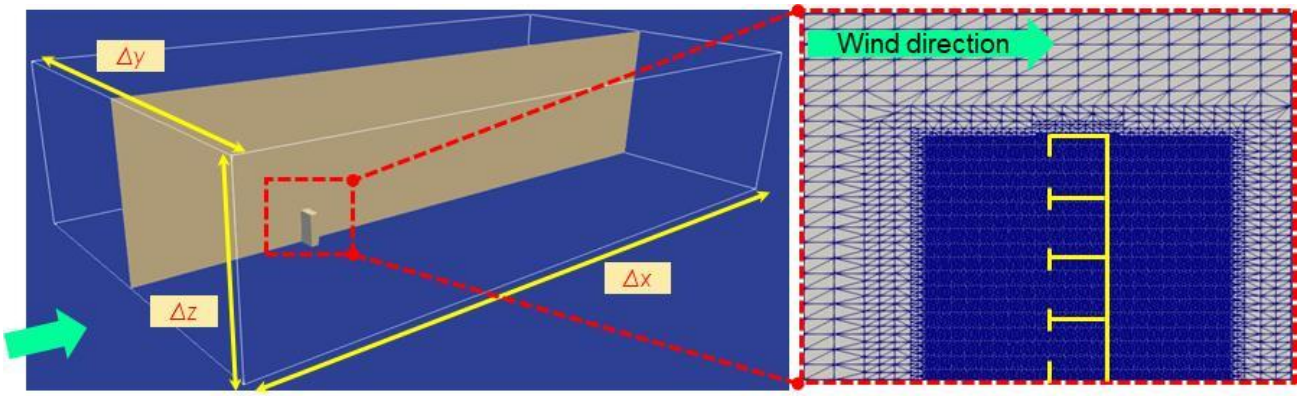

Fig. 12. Mesh distribution near the building and openings for the V2 level

3.3.1 Mean Velocity Profile

For further validation of the mean velocity profiles, in addition to the inlet velocity profile, several locations near the building were chosen according to the wind tunnel results of AIJ [5]. Figure 13 shows the three profile locations selected for validation with the CFD data. Point 1 is located at 50 mm upwind of the building, Point 2 is above the building's top surface and Point 3 is 50 mm downwind of the building.

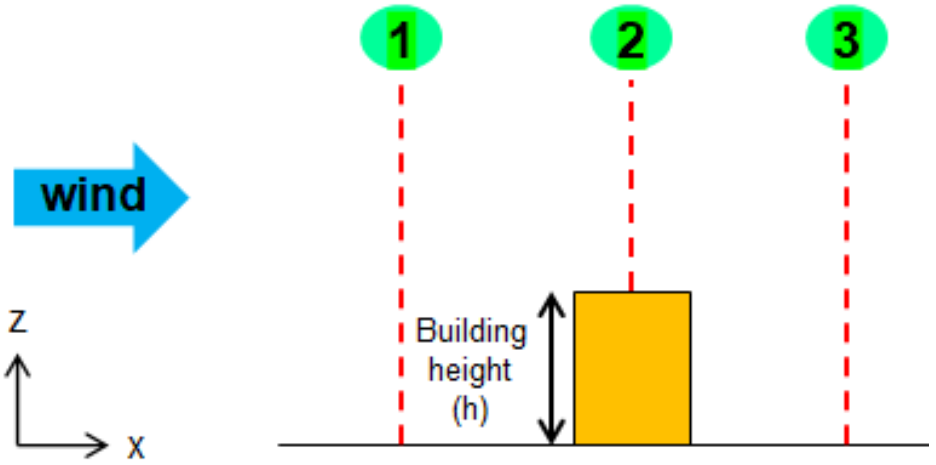

Fig. 13. Point locations selected for mean velocity profiles around the building

The mean velocity profiles of the three locations are shown in Figures 14. All selected profiles taken for all mesh refinement levels show high consistency with the wind tunnel data. Slight underestimation of the CFD results is seen in Figure 14(a) between z/h = 0 and z/h = 1.0. This is the region wherein the wind velocity slightly increases with height. Some backward flows which occur as a result of stagnation point that is present on the windward surface of the building, may also affect the accuracy of the simulation results. Nevertheless, the overall consistency observed in the figure indicates the accuracy of the RANS *k*-epsilon model adopted for the simulations in this study.

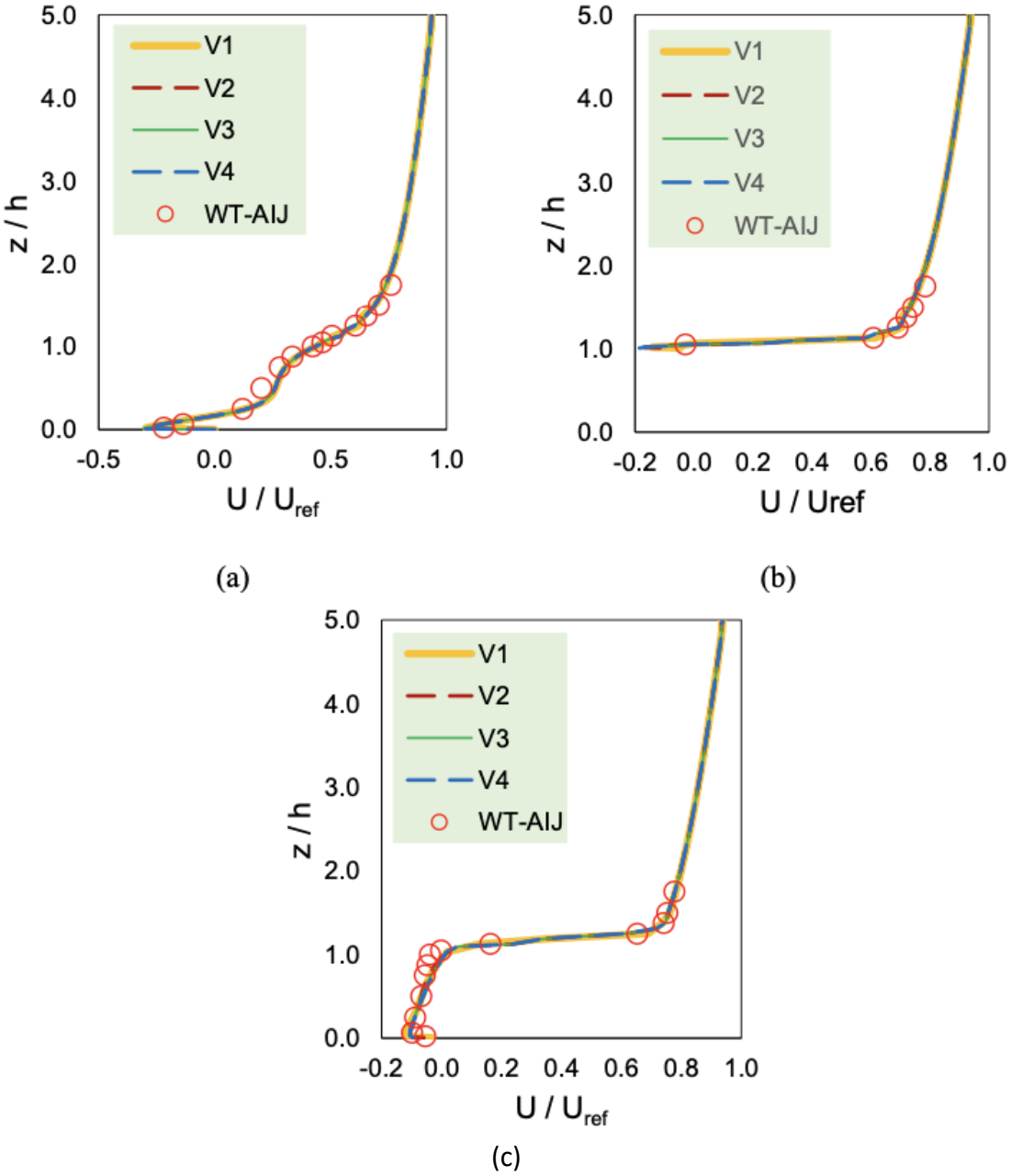

Fig. 14. Comparison of the mean velocity profiles between the different mesh refinement levels of the CFD simulations and the WT data from the AIJ database at three points: (a) Point 1, (b) Point 2 and (c) Point 3

3.3.2 Mean Ventilation Rate

Ventilation rate, Q was determined at each window opening of the building using the mean velocity data. Q was determined based on the single-sided ventilation which involves only one windward opening as used in the present simulations. The equation of the single-sided ventilation rate is as follows [3].

$$Q = 0.025AV \quad (1)$$

where, *A* is the area of the opening [m2] and *V* is the mean velocity magnitude [m/s] taken at the inlet of the opening. Figure 15 shows the comparison of mean ventilation rates obtained for each

refinement level relative to the highest refinement level, V4. The figure shows that the normalized ventilation rate increases to unity as the refinement level is increased. V3 has the highest accuracy with respect to V4, for which *Q*/*QV4* is 0.92 ± 0.10. Additionally, the coefficient of variation of the mean ventilation rates between V3 and V4 is less than 5 %, suggesting close similarity with V4. Hence, V3 was chosen for the second-stage simulation.

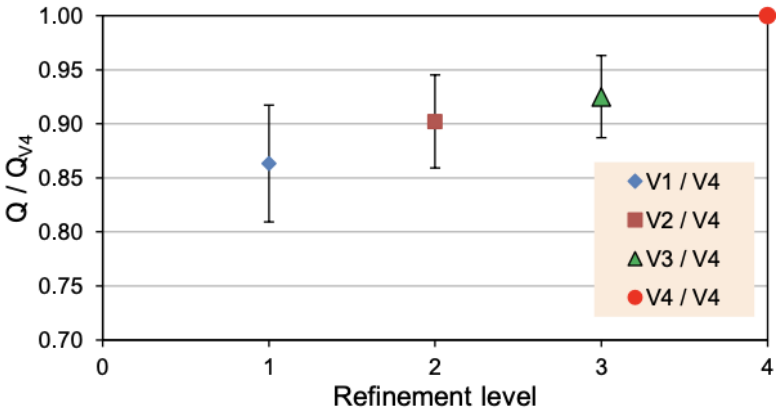

Fig. 15. Comparison of the mean velocity profiles between the different mesh refinement levels of the CFD

4. Results and Discussion

4.1 Step-Up Canyon Configuration

The simulation will be run for four types of building configurations with 3 variations of the window-to-wall ratios (WWRs). There are several step-up canyon configurations used in this study, as shown in Figure 16. The canyon with the same height of the upwind and the downwind buildings is categorized as a deep canyon (DC). The other three are step-up canyons, which are SU-75, SU-50 and SU-25; 'SU' refers to the step-up canyon while the number denotes the canyon's aspect ratio (e.g., '75' refers to the aspect ratio of 0.75). The window opening size was quantified by the WWR; for each simulation case, WWR = 0.25, which corresponds to the opening area, *A* of 0.98 × 10-3 m2, was used. The wind direction is set perpendicular towards the windward surface of the building.

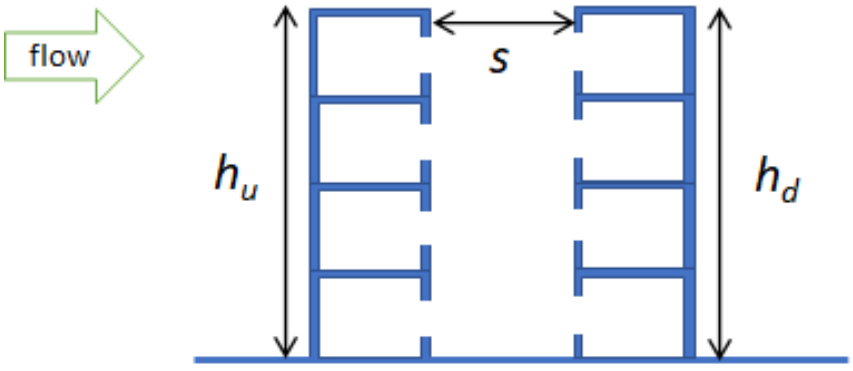

Fig. 16. Schematic of a street canyon where h_u is the height of the upwind building, h_d is the height of the downwind building and *s* is the distance between the two buildings

In addition, the dimensions of each configuration are presented in Table 3. The separation distance, s, between the two buildings is maintained for all cases. This is based on the study by Oke [17] that the occurrence of skimming flow is identified in a deep canyon wherein the separation

distance is equal to the building height; this was also observed through the RANS simulation of Zaki *et al*., [27]. Therefore, in this study the separation distance was maintained for all three step-up canyons, as was the downwind building height, *hd*, to investigate the flow improvement in the street canyon (from the skimming flow in the deep canyon) with respect to the decreasing upwind building height, hu and the street canyon's aspect ratio, *hu*/*hd*.

Table 3
Street canyon configuration

Configuration	h_u (m)	h_d (m)	s (m)	h_u/h_d
DC	0.20	0.20	0.20	1.00
SU-75	0.15			0.75
SU-50	0.10			0.50
SU-25	0.05			0.25

For a better illustration, Figure 17 shows the 3D schematics of all configurations with window openings on the upwind and downwind buildings.

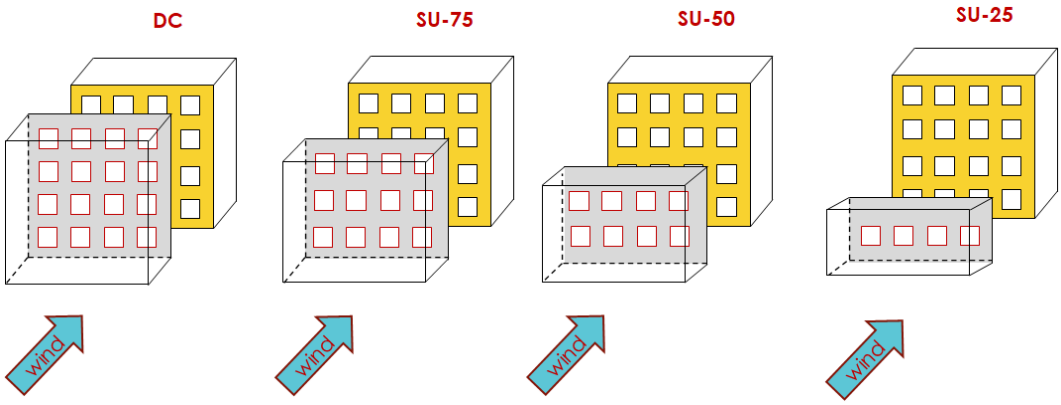

Fig. 17. 3D schematics of all street canyon configurations with window openings

4.2 Mean Flow Field

To obtain the mean flow fields of the simulation cases, an open-sourced program namely Paraview® was used. The output data produced by OpenFOAM was extracted and visualized Paraview. Figure 18 shows the mean velocity distribution and the mean pressure field in the street canyon region of SU-25. The figure shows the visualizations of mean velocity and pressure fields on a 2D plane at the centre of the computational domain. The blue region represents low velocities and low pressures while the red region is where the velocity and pressure are high. The wind flow direction is constituted with arrows; it can be seen that only a minimal amount of recirculating flow is observed in the street canyon, mainly below the height of the upwind building. The deflection of wind flow caused by the upwind building is not present and a downdraft of wind can be seen to form from the second floor flowing downwards.

In addition, the pressure distribution indicates higher values obtained near the downwind building and in the units of the top two floors. This is due to no sheltering from the upwind building which is relatively lower than the downwind building.

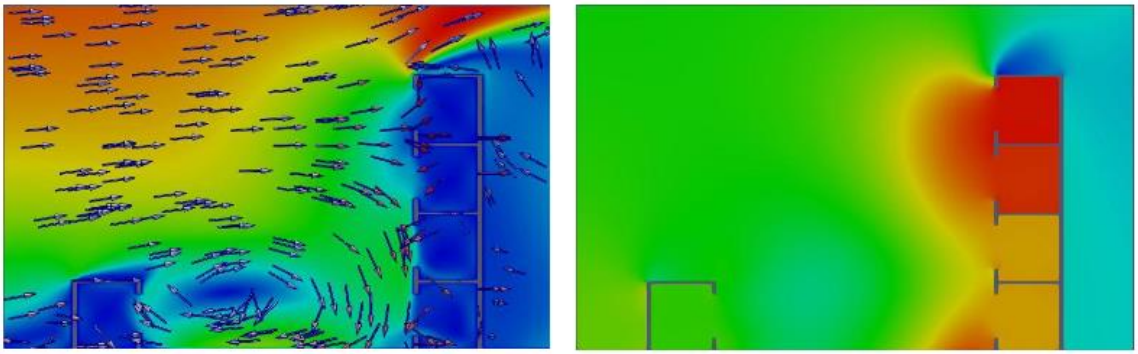

Fig. 18. Simulation results of SU-25 (a) Mean velocity distribution and (b) Mean pressure field

Figure 19 shows the mean velocity distribution and the mean pressure field in the street canyon region of SU-50. The visualization of the mean flow in this street canyon shows a formation of recirculating flow formed from the upwind building height. A downdraft is prominent from the second floor of the downwind building flowing towards the ground floor. Moreover, a deflected flow is formed due to the height of the upwind building which redirects the flow towards the second floor of the downwind building. This results in an expected higher ventilation rate than normal at the second floor as the green region can be noticeably seen flowing towards the opening; this is further discussed in the next section.

However, the pressure distribution is different from the SU-25 case. The figure indicates higher values obtained near the downwind building, but only at the topmost floor. This is due to sheltering effect of the upwind building which stands half the height of the downwind building. Hence, the sheltering effect is more significant in this configuration. This also means that wind-induced ventilation in lower floors (particularly the ground and first floors) of SU-50 is reduced relative to that can be generated in SU-25.

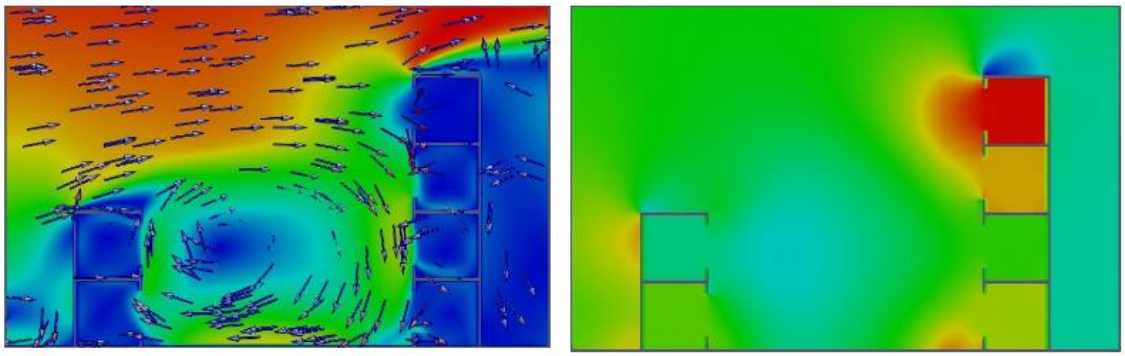

Fig. 19. Simulation results of SU-50 (a) Mean velocity distribution and (b) Mean pressure field

Lastly, Figure 20 shows the mean velocity distribution and the mean pressure field in the street canyon region of SU-75. In this configuration, the recirculating flow is the most apparent compared to the previous canyon configurations. The deflection flow which is denoted by the green region shows that it flows above and beyond the downwind building. Downdraft in this building configuration is very obvious as it is observed on the windward facade of the downwind building from the top floor towards the ground floor. It can be seen that in comparison with SU-25 and SU-

50, the canyon flow is characterized by lower velocity. This is almost similar to the occurrence of a skimming flow [17,26].

Furthermore, the pressure in the street canyon is uniformly low since the upwind building is almost the same height as the downwind building. This is important to show since it can perceived that the canyon flow for the SU-75 case has relatively lower velocity, and hence, resulting in low wind-induced ventilation. This is further discussed in the next section. It can also be seen that the windward façade of the upwind building experiences high pressure as the building blocks most of the incoming wind flow into the street canyon, creating a stagnation region in its vicinity.

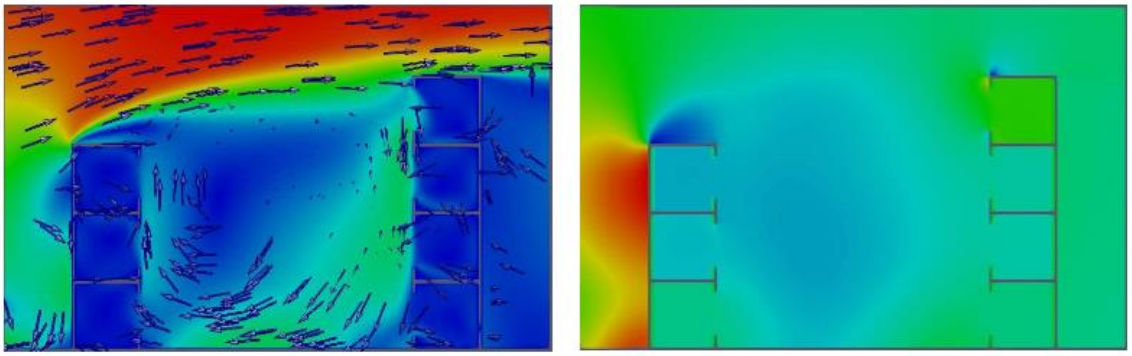

Fig. 20. Simulation results of SU-75 (a) Mean velocity distribution and (b) Mean pressure field

4.3 Mean Ventilation Rate

The mean ventilation rate, *Q* was calculated based on the equation by Allard [3] as presented as Eq. (1). Figure 21 illustrates the position of each opening at each floor of the downwind building. In this analysis, only the openings on a half of the building were selected due to the symmetry of simulated flows in the computational domain. The geometry of the building is also symmetrical in the spanwise direction. Moreover, only the window openings of the downwind building are taken for the calculation of the mean ventilation rate in this analysis. This is because the downwind building is directly affected by the street canyon's aspect ratio which changes from 1.0 - 0.25, corresponding to the decrease of the upwind building height.

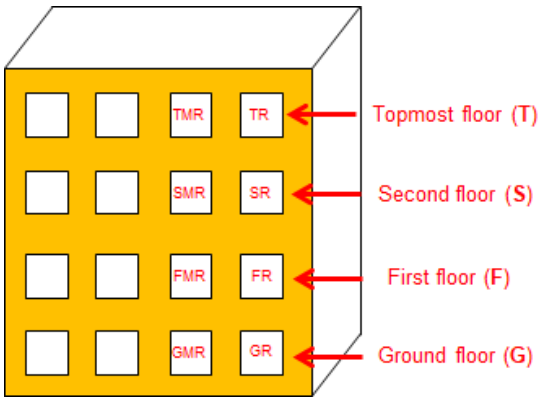

Fig. 21. Window openings on the windward façade of the downwind building

Figure 22 shows the results of the mean ventilation rate, *Q* of all openings shown in Figure 21, with respect to the street canyon's aspect ratio, h_u/h_d. A decreasing pattern is expected to be seen,

and is shown by the mean ventilation rates of the ground-floor openings, GMR and GR as the aspect ratio increases. In fact, the mean ventilation rates of all openings approach zero when h_u/h_d = 1.0 (deep canyon), suggesting the influence of skimming flow in minimizing wind-induced ventilation.

Anomalies in the results are shown when h_u/h_d = 0.5 at the openings (i.e. FMR, FR, SMR and SR) on the first and second floors. The mean ventilation rates are shown to increase for the SU-50 case. In fact, this phenomenon is explained in the previous section, regarding the mean flow distribution in the street canyon, wherein the deflected flow cause by the upwind building resulted in redirection of flow into the street canyon. This induces more flow particularly at the first and second floors of the downwind building, thereby increasing the mean ventilation rate. Another consequence of the deflected flow in the SU-50 case is the decrease of the mean ventilation rate at the topmost floor openings i.e. TMR and TR.

In general, a decreasing pattern of the mean ventilation rate is observed for most of the openings, especially from h_u/h_d = 0.50 to h_u/h_d = 1.0. This is a significant finding which has not been documented in previous studies.

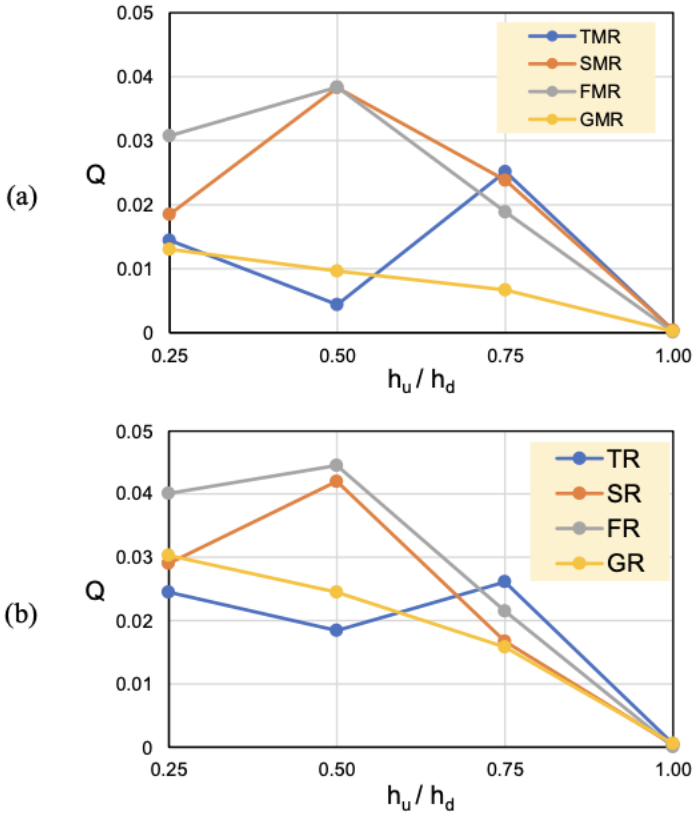

Fig. 22. Mean ventilation rate, Q versus the street canyon's aspect ratio, h_u/h_d

4.4 Ventilation Rate of the Ground-Floor Opening

In the previous section, it has been shown that the mean ventilation rates of the ground- floor openings, namely GR and GMR, are mostly affected by the increasing h_u/h_d. The focus on the ground-floor ventilation rate is due to it being the lowest level of the buildings which is most sheltered from the incoming wind. Therefore, to further demonstrate the influence of h_u/h_d on the mean ventilation rate, Figure 23 shows the mean ventilation rates of the two ground-floor openings for both upwind and downwind buildings.

Figure 23 shows that the ventilation rate increases significantly as the aspect ratio decreases from h_u/h_d = 1.0 (DC) to h_u/h_d = 0.25 (SU-25), mainly at the downwind building. The ventilation rate for the deep canyon can be observed to be almost zero while for the SU-25 configuration, the ventilation rate increases and exceeds 2.5 × 10-5 m3/s. At the upwind building, the increase of the ventilation rate is also observed, with slight discrepancy between h_u/h_d = 0.5 (SU-50) and h_u/h_d = 0.25 (SU-25). This result indicates that the skimming flow effect, which is normally present in a deep canyon, can be reduced when h_u/h_d is decreased; in other words, the skimming flow effect is effectively eliminated in step-up canyons.

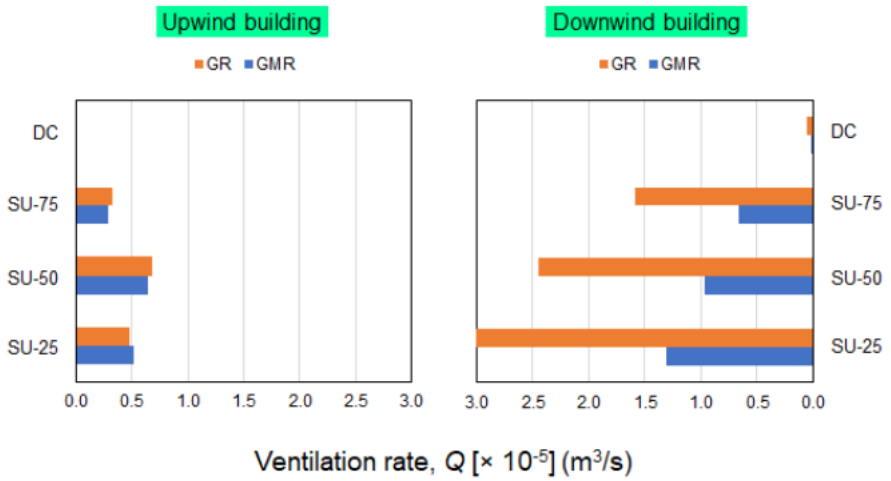

Fig. 23. Mean ventilation rates, *Q* of the ground-floor openings for both upwind and downwind building

5. Conclusions

The wind flow characteristics in the street canyons were shown to be influenced by the aspect ratio where the height of the upwind building influences the wind direction flowing into the street canyon. The higher the height of the upwind building, the less wind flow velocity in the street canyon. The step-up canyon was also shown to be effective at allowing more wind flow into the street canyon which results in an improved ventilation.

The results obtained from the CFD simulations indicated the suitability of the simulation settings used to resolve wind flows around the isolated building. The results were improved through the implementation of the grid sensitivity study wherein the mesh of the computational domain was refined. This was to ensure the mesh size applied in this research is adequate to produce accurate results. In addition, the CFD simulation results were validated against the published experimental data from the AIJ database. The validation demonstrated that the CFD simulation is a cost-effective and time-saving method compared to collecting experimental data from wind tunnel facilities.

References

[1] Addepalli, Bhagirath, and Eric R. Pardyjak. "Investigation of the flow structure in step-up street canyons—mean flow and turbulence statistics." *Boundary-layer meteorology* 148, no. 1 (2013): 133-155. https://doi.org/10.1007/s10546-013-9810-5

[2] Aflaki, Ardalan, Mahsan Mirnezhad, Amirhosein Ghaffarianhoseini, Ali Ghaffarianhoseini, Hossein Omrany, Zhi-Hua Wang, and Hashem Akbari. "Urban heat island mitigation strategies: A state-of-the-art review on Kuala Lumpur, Singapore and Hong Kong." *Cities* 62 (2017): 131-145. https://doi.org/10.1016/j.cities.2016.09.003

[3] Allard, Francis. "Natural ventilation in buildings. A design handbook." (1998).

[4] Ai, Z. T., and Cheuk Ming Mak. "Wind-induced single-sided natural ventilation in buildings near a long street canyon: CFD evaluation of street configuration and envelope design." *Journal of Wind Engineering and Industrial Aerodynamics* 172 (2018): 96-106. https://doi.org/10.1016/j.jweia.2017.10.024
[5] Architectural Institute of Japan. "AIJ Benchmarks for Validation of CFD Simulations Applied to Pedestrian Wind Environment Around Build." (2016).
[6] Assimakopoulos, Vasiliki D., H. M. ApSimon, and N. Moussiopoulos. "A numerical study of atmospheric pollutant dispersion in different two-dimensional street canyon configurations." *Atmospheric Environment* 37, no. 29 (2003): 4037-4049. https://doi.org/10.1016/S1352-2310(03)00533-8
[7] Caciolo, Marcello, Pascal Stabat, and Dominique Marchio. "Numerical simulation of single-sided ventilation using RANS and LES and comparison with full-scale experiments." *Building and Environment* 50 (2012): 202-213. https://doi.org/10.1016/j.buildenv.2011.10.017
[8] Derakhshan, Shahram, and Ahmad Shaker. "Numerical study of the cross-ventilation of an isolated building with different opening aspect ratios and locations for various wind directions." *International Journal of Ventilation* 16, no. 1 (2017): 42-60. https://doi.org/10.1080/14733315.2016.1252146
[9] Dhalluin, Adrien, and Emmanuel Bozonnet. "Urban heat islands and sensitive building design–A study in some French cities' context." *Sustainable Cities and Society* 19 (2015): 292-299. https://doi.org/10.1016/j.scs.2015.06.009
[10] Ai, Z. T., and Cheuk Ming Mak. "CFD simulation of flow in a long street canyon under a perpendicular wind direction: Evaluation of three computational settings." *Building and Environment* 114 (2017): 293-306. https://doi.org/10.1016/j.buildenv.2016.12.032
[11] Fernández, Francisco J., Lino J. Alvarez-Vázquez, N. García-Chan, Aurea Martínez, and Miguel E. Vázquez-Méndez. "Optimal location of green zones in metropolitan areas to control the urban heat island." *Journal of Computational and Applied Mathematics* 289 (2015): 412-425. https://doi.org/10.1016/j.cam.2014.10.023
[12] Guo, Penghua, Shuang Wang, Ben Xu, Qinglong Meng, and Yuan Wang. "Reduced-scale experimental model and numerical investigations to buoyance-driven natural ventilation in a large space building." *Building and Environment* 145 (2018): 24-32. https://doi.org/10.1016/j.buildenv.2018.09.019
[13] Ikegaya, Naoki, C. Hirose, Aya Hagishima, and Jun Tanimoto. "Effect of turbulent flow on wall pressure coefficients of block arrays within urban boundary layer." *Building and Environment*100 (2016): 28-39. https://doi.org/10.1016/j.buildenv.2016.02.005
[14] Levermore, Geoff, John Parkinson, Kwanho Lee, Patrick Laycock, and Sarah Lindley. "The increasing trend of the urban heat island intensity." *Urban climate* 24 (2018): 360-368. https://doi.org/10.1016/j.uclim.2017.02.004
[15] Li, Ju, Mingyu Zhou, Donald H. Lenschow, Zhigang Cheng, and Youjun Dou. "Observed relationships between the urban heat island, urban pollution island, and downward longwave radiation in the Beijing area." *Earth and Space Science* 7, no. 6 (2020): e2020EA001100. https://doi.org/10.1029/2020EA001100
[16] Mohajerani, Abbas, Jason Bakaric, and Tristan Jeffrey-Bailey. "The urban heat island effect, its causes, and mitigation, with reference to the thermal properties of asphalt concrete." *Journal of environmental management* 197 (2017): 522-538. https://doi.org/10.1016/j.jenvman.2017.03.095
[17] Oke, T. R. *Boundary Layer Climates* (2nd Edition). Abingdon, Oxon: Routledge. 1987.
[18] Orme, M. "Estimates of the energy impact of ventilation and associated financial expenditures." *Energy and Buildings* 33, no. 3 (2001): 199-205. https://doi.org/10.1016/S0378-7788(00)00082-7
[19] Qaid, Adeb, Hussanudin Bin Lamit, Dilshan Remaz Ossen, and Raja Nafida Raja Shahminan. "Urban heat island and thermal comfort conditions at micro-climate scale in a tropical planned city." *Energy and Buildings* 133 (2016): 577-595. https://doi.org/10.1016/j.enbuild.2016.10.006
[20] Santamouris, M. "Analyzing the heat island magnitude and characteristics in one hundred Asian and Australian cities and regions." *Science of the Total Environment* 512 (2015): 582-598. https://doi.org/10.1016/j.scitotenv.2015.01.060
[21] Shirzadi, Mohammadreza, Parham A. Mirzaei, and Mohammad Naghashzadegan. "Development of an adaptive discharge coefficient to improve the accuracy of cross-ventilation airflow calculation in building energy simulation tools." *Building and Environment* 127 (2018): 277-290. https://doi.org/10.1016/j.buildenv.2017.10.019
[22] Tominaga, Yoshihide, Akashi Mochida, Ryuichiro Yoshie, Hiroto Kataoka, Tsuyoshi Nozu, Masaru Yoshikawa, and Taichi Shirasawa. "AIJ guidelines for practical applications of CFD to pedestrian wind environment around buildings." *Journal of wind engineering and industrial aerodynamics* 96, no. 10-11 (2008): 1749-1761. https://doi.org/10.1016/j.jweia.2008.02.058
[23] United Nations, Department of Economic and Social Affairs, Population Division (2019). *World Population Prospects: The 2019 Revision, Highlights (ST/ESA/SER.A/423).*

[24] van Hooff, Twan, Bert Blocken, and Yoshihide Tominaga. "On the accuracy of CFD simulations of cross-ventilation flows for a generic isolated building: Comparison of RANS, LES and experiments." *Building and Environment* 114 (2017): 148-165. https://doi.org/10.1016/j.buildenv.2016.12.019

[25] Wong, Paulina Pui-Yun, Poh-Chin Lai, Chien-Tat Low, Si Chen, and Melissa Hart. "The impact of environmental and human factors on urban heat and microclimate variability." *Building and Environment* 95 (2016): 199-208. https://doi.org/10.1016/j.buildenv.2015.09.024

[26] Zaki, S. A., Hagishima, A., Tanimoto, J. (2012) 'Experimental study of wind-induced ventilation in urban buildings of cube arrays with various layouts', *Journal of Wind Engineering and Industrial Aerodynamics*, 103, pp. 31-40. https://doi.org/10.1016/j.jweia.2012.02.008

[27] Zaki, Sheikh Ahmad, Ahmad Zaki Jaafar, Ahmad Faiz, M. S. M. A. Mohammad, and A. A. Razak. "Investigation of surface roughness impact on mean wind flow using RNG k-ε model." *Jurnal Teknologi* 78, no. 9 (2016): 21-28. https://doi.org/10.11113/jt.v78.5161

[28] http://coolparramatta.com.au/about_us.